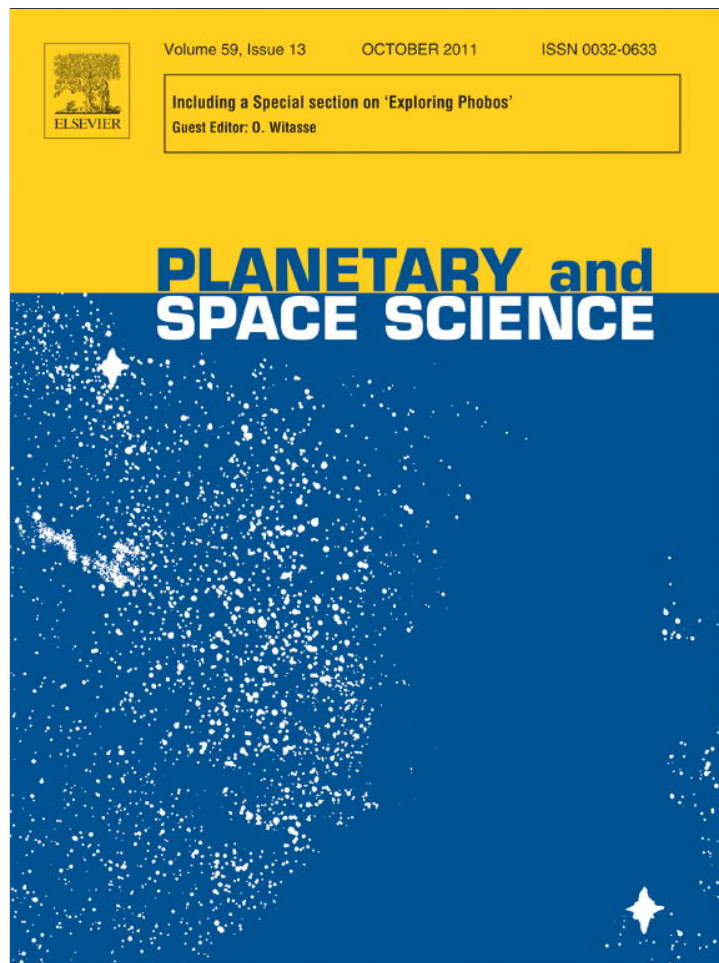


Provided for non-commercial research and education use.
Not for reproduction, distribution or commercial use.



This article appeared in a journal published by Elsevier. The attached copy is furnished to the author for internal non-commercial research and education use, including for instruction at the authors institution and sharing with colleagues.

Other uses, including reproduction and distribution, or selling or licensing copies, or posting to personal, institutional or third party websites are prohibited.

In most cases authors are permitted to post their version of the article (e.g. in Word or Tex form) to their personal website or institutional repository. Authors requiring further information regarding Elsevier's archiving and manuscript policies are encouraged to visit:

<http://www.elsevier.com/copyright>



Contents lists available at ScienceDirect

Planetary and Space Science

journal homepage: www.elsevier.com/locate/pss

The effect of Nix and Hydra on the putative Pluto–Charon dust cloud

Andrew Poppe^{a,b,1,*}, Mihály Horányi^{a,b}^a Laboratory for Atmospheric and Space Physics, University of Colorado, UCB 392, Boulder, CO 80303, USA^b Department of Physics, University of Colorado, Boulder, CO 80309, USA

ARTICLE INFO

Article history:

Received 6 April 2011

Received in revised form

30 July 2011

Accepted 1 August 2011

Available online 6 August 2011

Keywords:

Pluto

Charon

Nix

Hydra

Dust clouds/rings

ABSTRACT

Impact-generated dust clouds around airless bodies have been observed or suggested to be present throughout the solar system, including around the Martian, Galilean and Saturnian satellites. Simulations have assessed Pluto and Charon as sources of a possible dust cloud or torus and found that such a cloud would be dominated by Charon-produced ejecta and would have an optical depth of $\tau \approx 10^{-11}$. These simulations were conducted before the discovery of two additional, small satellites of Pluto, Nix and Hydra. These small moons may yield impact-generated dust in excess of their larger counterparts due to their lower escape velocities, despite their smaller cross sections. In this paper, we extend a previous model of the Pluto–Charon dust cloud to include Nix and Hydra, both as sinks for Pluto- and Charon-generated dust and as sources of impact-generated dust. We find that Nix- and Hydra-generated dust grains outlive Pluto and Charon dust grains significantly and are the dominant contributors of dust in the Pluto–Charon system. Furthermore, we estimate the net geometric optical depth of grains between 0.1 and 100 μm to be on the order of 10^{-7} .

© 2011 Elsevier Ltd. All rights reserved.

1. Introduction and previous work

Airless bodies throughout the solar system are exposed to continual bombardment by interplanetary micrometeorites. These micron and sub-micron sized grains produce large amounts of impact-generated ejecta, forming debris clouds or rings. Examples of this process are expected to exist at or have been found at the Martian moons (Ip and Banaszekiewicz, 1990; Juhász and Horányi, 1995), the minor and Galilean satellites of Jupiter (Burns et al., 1999; Krüger et al., 1999, 2000; Krivov et al., 2002), and the Saturnian satellites (Hedman et al., 2009; Verbischer et al., 2009). These rings or tori are often extremely sparse, with optical densities, $\tau < 10^{-5}$, making ground-based optical detection difficult. Given the ubiquity of impact-generated dust clouds and rings throughout the solar system, it is natural to expect that a similar effect is present in the Pluto–Charon system (Thiessenhusen et al., 2002). Previous work has investigated the possibility of an impact-generated dust cloud around Pluto and Charon via both simulation and observation (Thiessenhusen et al., 2002; Steffl and Stern, 2007). By assuming typical values for the interplanetary micrometeorite flux and the impact ejecta yield, mass and speed distributions, the Pluto–Charon system can be modeled via a particle-tracing code. Previous simulations,

completed before the discovery of Pluto's additional small satellites, Nix and Hydra, found that between Pluto and Charon, dust grains launched from Charon have much longer lifetimes and therefore, represent a greater contribution to the Pluto–Charon dust cloud than do Pluto-ejected grains (Thiessenhusen et al., 2002). The net optical depth for the cloud was predicted to be $\tau \approx 10^{-11}$, far too low to be observed optically.

Following the discovery of Nix and Hydra (Weaver et al., 2006; Steffl et al., 2006), observations of the Pluto system with the Hubble Space Telescope were analyzed and did not detect any dust rings or clouds (Steffl and Stern, 2007). Correspondingly, an upper limit was placed on the optical density of any such cloud at $\tau \approx 5 \times 10^{-5}$. An additional theoretical estimate for the optical depth of any rings or dust clouds, including the presence of Nix and Hydra, was derived at, $\tau \approx 10^{-6}$, with the assumption that the grain lifetimes from Nix and Hydra were on the order of 10^5 year (Stern et al., 2006).

In order to investigate the role that Nix and Hydra play in the generation of a dust cloud in the Pluto–Charon system, we have extended an earlier simulation model to include these small moons as both potential sinks and sources of dust grains (Thiessenhusen et al., 2002). In Section 2, we evaluate a theoretical dust production rate for all four bodies in order to assess Nix and Hydra's ability to contribute dust relative to Pluto and Charon. In Sections 3 and 4, we describe the nature of the simulation and the results for all four bodies, respectively, including a prediction of the optical depth of the Pluto–Charon dust cloud and a prediction for the impact flux of grains onto the New Horizons spacecraft as it crosses the Pluto–Charon system in mid-2015 (Stern, 2008). We conclude and discuss further areas of research in Section 5.

* Corresponding author at: Space Sciences Laboratory, 7 Gauss Way, University of California at Berkeley, Berkeley, CA 94720, USA.

E-mail address: poppe@ssl.berkeley.edu (A. Poppe).

¹ Now at: Space Sciences Laboratory, 7 Gauss Way, University of California at Berkeley, Berkeley, CA 94720, USA.

2. Dust production rates

The dust grain production rate from each body in the Pluto–Charon system, now including Nix and Hydra, can be estimated, with relevant quantities listed in Table 1 (Thiessenhusen et al., 2002). As discussed in Thiessenhusen et al. (2002), the interplanetary dust flux at the orbit of Pluto has not yet been measured; however, previous work, using measurements from the Pioneer 10 and 11 meteoroid detectors, has partially constrained the dust flux at Pluto (Humes, 1980; Landgraf et al., 2002). In addition, recent measurements of the interplanetary dust flux inside 20 AU by the Student Dust Counter onboard New Horizons are currently being analyzed in order to constrain the dust density throughout the outer solar system (Horányi et al., 2008; Poppe et al., 2010). Upon completion of this study, an updated dust flux at Pluto can be used to further refine our results. Noting this important caveat, we follow previous work and calculate the interplanetary dust mass flux to each body using the impact speed, the interplanetary dust flux and the surface areas for all four bodies (Grün et al., 1985; Tholen et al., 2008). Using the calculated interplanetary grain impact speed for each body (row 4 of Table 1), and assuming a typical interplanetary impactor mass of $m = 10^{-14}$ kg and icy surfaces on all four bodies, the ejecta yield is estimated at $Y \approx 10$ (Koschny and Grün, 2001a). The ejecta mass distribution is governed by a power-law distribution of the form (adapted from Thiessenhusen et al. (2002))

$$N^+(> m) = \frac{1-\alpha}{\alpha} \frac{m^+}{m_{max}} \left(\frac{m}{m_{max}} \right)^{-\alpha}, \quad (1)$$

where m^+ is the total amount of ejected mass and m_{max} is the maximum ejected particle mass. Converting to the ejecta mass production rate gives

$$\frac{N^+(> m)}{1 \text{ s}} = Nm^{-\alpha}, \quad (2)$$

where N is a normalization constant. We follow the assumptions of the previous simulation and use values of $\alpha = 0.83$ and $m_{max} = 10^{-5}$ kg (Koschny and Grün, 2001b; Thiessenhusen et al., 2002). Listed in row 7 of Table 1 are the respective values for N for all four bodies.

The ejecta speed distribution, $f(u)$, is assumed to follow a power-law distribution of

$$f(u) = \frac{\gamma}{u_0} \left(\frac{u}{u_0} \right)^{-\gamma-1}, \quad (3)$$

where u is the launch velocity, u_0 is the lower cutoff velocity and $\int_{u_0}^{\infty} f(u) du = 1$ (Stöffler et al., 1975; Hartmann, 1985; Krivov et al., 2003). For the hard, icy surfaces of Pluto and its moons, typical values are $\gamma = 1.9$ and $u_0 = 40$ m/s (Frisch, 1992). Finally, the net mass escape rate is given by, $N_{esc}^+ = N^+ \int_{u_{esc}}^{\infty} f(u) du$, and is listed in Table 1 for all four bodies for three different grain sizes: 0.5 μm ,

5.0 μm , 50.0 μm (5.2×10^{-16} kg, 5.2×10^{-13} kg, 5.2×10^{-10} kg, assuming a density of ice). The net escape rates for Nix and Hydra are comparable to those of Pluto and Charon across all three sizes, highlighting the role that small bodies can play in generating dust clouds, tori and rings. The extremely low escape velocities of Nix and Hydra effectively compensate for their small cross-sections. While the net mass escape rates may be fairly even across all four bodies, the particle lifetimes from each body and at each size can be vastly different.

3. Dust dynamics

The equation of motion for a dust grain in the Pluto–Charon system with mass, m_d , is given by

$$m_d \ddot{\vec{r}} = \vec{F}_p + \vec{F}_c + \vec{F}_n + \vec{F}_h + \frac{\vec{I}_{\odot}}{d_p^2} \frac{\pi a^2}{c}, \quad (4)$$

where $\ddot{\vec{r}}$ is the grain's net acceleration and \vec{F}_i is the gravitational force from Pluto ($i=p$), Charon ($i=c$), Nix ($i=n$) and Hydra ($i=h$), respectively. Additionally, solar radiation pressure is included, where \vec{I}_{\odot} is the solar flux at 1 AU, c is the speed of light, d_p is the heliocentric distance of Pluto (in AU), and a is the grain radius. Radiation pressure shortens grain lifetimes by increasing the eccentricity of the grains' orbits and raising the likelihood of a close encounter and subsequent ejection from the Pluto–Charon system (Burns et al., 2001). The Lorentz force due to the interaction between charged grains and Pluto's hypothetical magnetosphere may also be an important effect to include; however, little is currently specifically known about Pluto's electromagnetic environment and simulations have shown a wide degree of variability (Delamere and Bagenal, 2004; Harnett et al., 2005; Delamere, 2009), and therefore, we do not include such an effect at this time. Observations by the Solar Wind Around Pluto (SWAP) instrument onboard the New Horizons mission during its 2015 fly-by of the Pluto–Charon system will yield significant knowledge of the Pluto electromagnetic environment and will allow future modeling to include the Lorentz force (McComas et al., 2008). Additionally, we neglect Poynting–Robertson drag, which at the heliocentric distance of Pluto is many orders of magnitude less than local gravitational forces and therefore has timescales much longer than typical grain lifetimes in the Pluto–Charon system (Burns et al., 1979).

For each body, the trajectories of grains at three different sizes (0.5 μm , 5.0 μm , 50.0 μm or 5.2×10^{-16} kg, 5.2×10^{-13} kg, 5.2×10^{-10} kg, assuming a density of ice) were integrated until they either impacted Pluto or one of its moons, or reached the Pluto Hill radius ($\approx 6000R_p$). For the 0.5 and 5.0 μm cases, 2500 grains were simulated for each body, while for the 50.0 μm case, 500 grains were used. In order to assess the effect that Nix and

Table 1
Values used in estimating the dust grain production rates for Pluto, Charon, Nix and Hydra.

	Pluto	Charon	Nix	Hydra
Radius (km)	1147	606	44	36
Mass (kg)	1.304×10^{22}	1.52×10^{21}	5.8×10^{17}	3.2×10^{17}
Escape velocity (m/s)	1231	579	42	34
Grain impact speed (m/s)	3250	2950	2230	2100
Mass impact rate (kg/s)	2.15×10^3	5.4×10^2	2.2	1.4
Ejecta production rate (kg/s)	2.15×10^4	5.47×10^3	22	14
N (s^{-1}) (see Eq. (2))	9.6	2.45	9.9×10^{-3}	6.1×10^{-3}
$\int_{u_{esc}}^{\infty} f(u) du$ (see Eq. (3))	1.48×10^{-3}	6.23×10^{-3}	0.911	1.00
$N_{esc}(m > 5.2 \times 10^{-16} \text{ kg})$ (s^{-1})	1.87×10^8	1.99×10^8	1.11×10^8	0.80×10^8
$N_{esc}(m > 5.2 \times 10^{-13} \text{ kg})$ (s^{-1})	6.05×10^5	6.50×10^5	3.58×10^5	2.59×10^5
$N_{esc}(m > 5.2 \times 10^{-10} \text{ kg})$ (s^{-1})	1.96×10^3	2.09×10^3	1.16×10^3	0.84×10^3

Hydra might have as sinks for Pluto- and Charon-generated dust grains, an additional set of simulations was run for Pluto and Charon without the presence of Nix and Hydra for 0.5 μm grains. Dust grains were launched from random positions on Pluto and its moons, with a random launch angle inside a cone of $\theta < 45^\circ$ from the surface normal. The launch velocity of each grain was randomly assigned between 0.7 and 2.0 times the relevant escape velocity, representing the portion of the ejecta velocity distribution that contributes most to the density of orbiting grains (i.e., slower grains remain gravitationally bound to the body while faster grains rapidly leave the Pluto system).

4. Results

For each grain, the position and velocity are tracked through its lifetime and from these values, the orbital elements in the barycentric frame can be calculated. Fig. 1 shows the barycentric distance and orbital elements for a typical 0.5 μm grain from Nix with an initial launch velocity, $v = 1.44v_N$, where v_N is the Nix escape velocity. The orbital elements show significant structure and periodicity, due to repeated close encounters with Pluto, Charon and Nix. For example, Fig. 2 shows the distance from the grain to Nix over the lifetime of the grain. Eventually, the grain gains enough orbital energy to escape the Pluto system entirely due to repeated close encounters.

4.1. Lifetimes

Fig. 3(a)–(c) shows the average lifetime versus normalized escape velocity for the three grain sizes launched from all four bodies, including the presence of Nix and Hydra. Additionally, results for grains launched from Pluto and Charon without the presence of Nix and Hydra are also shown for the 0.5 μm case. In this case, the presence of the two small, additional moons did not

significantly change the average lifetime of the Pluto- and Charon-ejected grains, mainly due to the relatively small mass and cross-sections of Nix and Hydra. In all cases, a distinct jump is seen as the normalized launch velocity transitions above unity, corresponding to the transition from ballistic, bound trajectories of grains that rapidly re-impact the bodies, to grains that are ejected into the Pluto–Charon system and beyond. In comparison with previous simulation results, the lifetimes of Pluto- and Charon-generated grains are roughly a factor of five shorter, due to the inclusion of solar radiation pressure (Thiessenhusen et al., 2002).

For Nix and Hydra, the average lifetimes for grains with launch velocities greater than the respective escape velocity are between one and four orders-of-magnitude longer than those for Pluto or

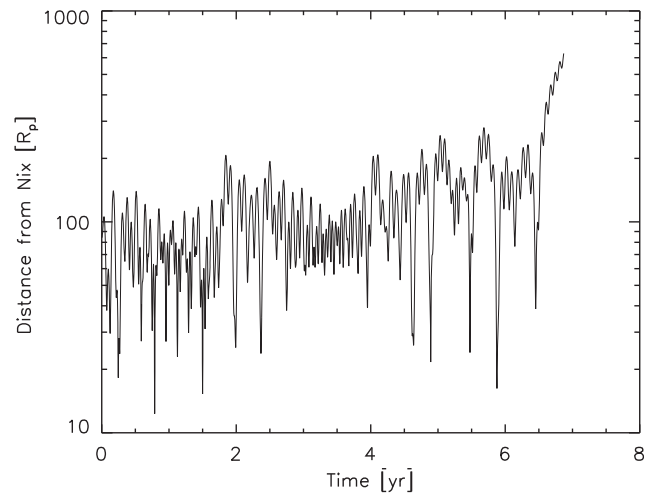


Fig. 2. The distance to Nix for the grain shown in Fig. 1.

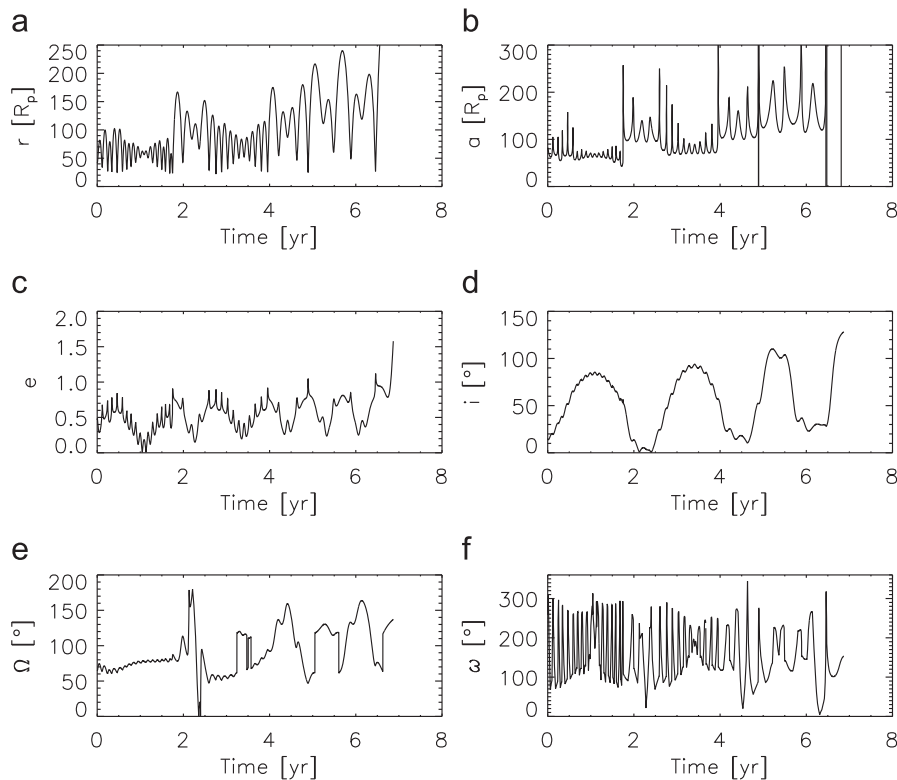


Fig. 1. The orbital elements for one grain launched from Nix. Shown as a function of time are (a) barycentric distance [R_p], (b) semi-major axis [R_p], (c) eccentricity, (d) inclination, (e) longitude of ascending node and (f) argument of pericenter.

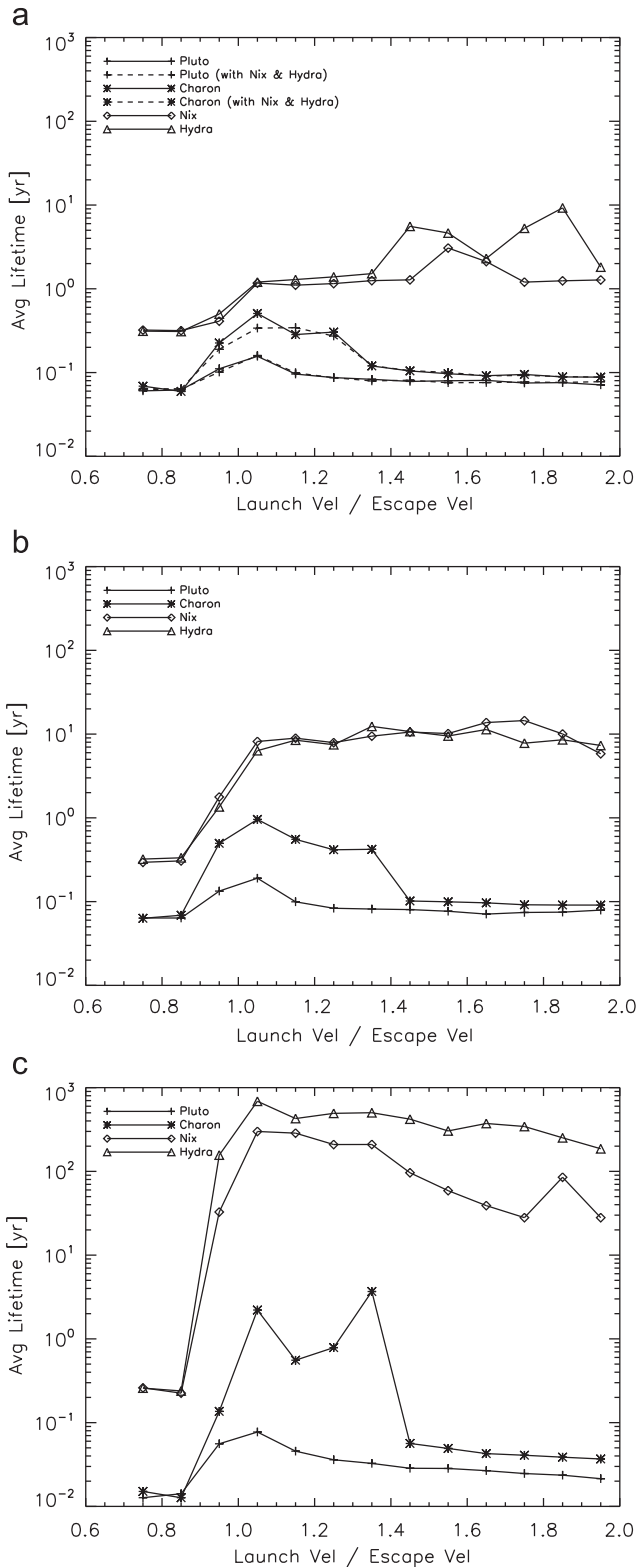


Fig. 3. The average grain lifetime for all three grain sizes versus normalized launch velocity for all four bodies, respectively. Additionally, the results for Pluto and Charon without the presence of Nix and Hydra are shown for 0.5 μm grains, with no appreciable change. (a) 0.5 μm, (b) 5.0 μm and (c) 50.0 μm.

Charon, with larger grains having longer lifetimes. The increase in Nix and Hydra grain lifetime as a function of particle size is due to the decreasing relative strength of solar radiation pressure for larger grains. The orbits of the 0.5 μm grains are easily perturbed by solar radiation pressure which increases the likelihood of a

close encounter and subsequent ejection by one of the other bodies, while the larger grains maintain relatively stable orbits and are therefore less susceptible to such scattering. Despite the relative increase in lifetimes for larger grains, we find that the lifetimes for all grains are significantly less than the theoretical moon–grain collision lifetimes using Eq. (1) from Hamilton and Burns (1994) (for example, the collision lifetimes of 50.0 μm grains from Nix and Hydra are estimated at 6000 and 23,000 years, respectively). In fact, we see that the dominant loss mechanism for Nix and Hydra grains across all sizes with launch velocities greater than the respective escape velocity is ejection from the system, rather than re-collision with their parent moon.

A qualitative explanation for the relative increase in Nix and Hydra lifetimes with respect to Pluto and Charon across all sizes may be found in a comparison of the body escape velocities and system escape velocities for each moon. Table 2 lists the body escape velocity, the average orbital velocity and the system escape velocity, respectively, for each body. Grains launched from each moon possess not only their escape velocity but also the orbital velocity of the moon about the barycenter. For Pluto and Charon, the required escape velocity for dust grains, in addition to the orbital velocity, is enough to overcome the entire system escape velocity. In contrast, the sum of the escape and orbital velocities for Nix and Hydra, respectively, is not large enough to overcome the system escape velocity (even in the maximum case when a grain is ejected directly along the orbital velocity vector). Thus, there exists a range in launch velocity space for Nix and Hydra where grains are easily ejected from the moon itself, but not from the Pluto system as a whole.

4.2. Inter-body grain transport

Dust grains in the Pluto–Charon system have two basic loss mechanisms: collision with another body in the system, whether the parent body or another, and dynamical escape from the system entirely. When a grain satisfies either of these conditions (impact or escape), the simulation is halted for that grain and the loss mechanism is noted. Using this data, a transfer matrix can be constructed for grains from each body. Shown in Table 3 is the percentage of grains that were transported from one body to another, as well as the percentage of grains that escaped the system, as a function of their parent body for each of the modeled grain sizes. Grains with launch velocities less than their respective escape velocity were excluded from this analysis in order to focus on the population of grains that can dynamically reach the other bodies in the system.

For Pluto and Charon, almost all grains across all three sizes escape from the system due to their high ejection velocity relative to the entire Pluto–Charon system escape velocity. No grains from Pluto or Charon of any size impact Nix or Hydra, due to the extremely small cross-sections of these two moons. In contrast, Nix and Hydra have a much larger percentage of grains that collide with either Pluto or Charon. Commensurate with this, the escape percentages for Nix and Hydra are significantly lower than those for Pluto and Charon. As the grain size increases, transfer from Nix and Hydra to Pluto and Charon decreases, and transfer between Nix and Hydra increases, due to the more tightly bound

Table 2
Various velocities for Pluto, Charon, Nix and Hydra.

	Pluto	Charon	Nix	Hydra
Body escape velocity (m/s)	1231	579	42	34
Co-orbital velocity (m/s)	23.5	199	142	122
System escape velocity (m/s)	1231	658	193	191

orbits of larger grains from Nix and Hydra. Correspondingly, escape percentages for Nix and Hydra grains decrease with increasing grain size, as Nix and Hydra become greater particle sinks. The significant amount of grain transfer from Nix and Hydra to Pluto and Charon (as well as transfer from Charon to Pluto) could result in deposition of grains on the surfaces of Pluto and Charon (Stern, 2009), similar to that found on Iapetus in the Saturnian system (Cruikshank et al., 1983; Porco et al., 2005; Hendrix and Hansen, 2008; Verbischer et al., 2009); however, volatile transport on Pluto may act to resurface and effectively erase any such signature on Pluto (Stern et al., 1988; Spencer et al., 1997).

Table 3

The percentage of dust grains transferred from one body to another or that escaped, for grains with launch velocities greater than or equal to their respective moon's escape velocity. Results are shown for all three modeled dust grain sizes, 0.5, 5.0 and 50.0 μm .

	Pluto	Charon	Nix	Hydra	Escape
0.5 μm					
Pluto	0.24	0.02	0.00	0.00	99.7
Charon	7.22	1.58	0.00	0.00	99.2
Nix	7.43	16.1	1.73	0.00	74.7
Hydra	5.93	10.5	0.00	4.25	79.4
5.0 μm					
Pluto	0.24	0.00	0.00	0.00	99.8
Charon	4.89	2.37	0.00	0.00	92.7
Nix	5.03	13.8	3.20	0.00	77.9
Hydra	4.05	9.53	0.00	5.85	80.5
50.0 μm					
Pluto	0.60	0.00	0.00	0.00	99.4
Charon	8.03	0.91	0.00	0.00	91.1
Nix	3.95	8.58	28.8	0.48	58.2
Hydra	1.21	4.08	2.75	26.8	65.2

4.3. Optical depth

The optical depth of the Pluto–Charon dust cloud can be estimated using the trajectories from the simulation, which are sampled regularly. For each body, all grain trajectories are first weighted by the ejecta speed distribution, $f(u)$, and then used to update a $150 \times 150 \times 150 R_p$ array of the amount of time each grain spends in each unit of volume, $t_j(x,y,z)$, where j indexes each grain, with a $1 R_p$ resolution covering the Pluto–Charon system. The physical grain density for each body, $n_i(x,y,z)$, in the Pluto–Charon system is given by

$$n_i(x,y,z) = \frac{\sum_{j=1}^S t_j(x,y,z)}{S \times V} N_{p,i} \int_{0.7v_{esc,i}}^{2.0v_{esc,i}} f(u) du, \quad (5)$$

where $N_{p,i}$ is the physical number production rate estimated in Section 2, S is the total number of simulated grains, $V = R_p^3$ is the volume of an individual box and the integral over $f(u)$ represents the fraction of grains launched within the selected simulated ejecta velocity range (Thiessenhusen et al., 2002). In order to correctly account for the optical depth produced by grains over a wide range of sizes, we calculate the production rate for each of the three simulation grain radii, 0.5, 5.0, and 50.0 μm , using bounds of 0.1–1.0 μm , 1.0–10.0 μm , and 10.0–100.0 μm , respectively.

The geometric optical depth for an individual body, τ_i , is given by

$$\tau_i = \pi a^2 \ell \sum_{j=\ell_-}^{\ell_+} n_i(x,y_j,z), \quad (6)$$

where a is the grain radius, ℓ_+ and ℓ_- are the simulation bounds in y , and $\ell \equiv \ell_+ - \ell_-$. Fig. 4 shows the column density for 5.0 μm grains for each body normalized to its own respective maximum column density, in the frame as seen by the New Horizons

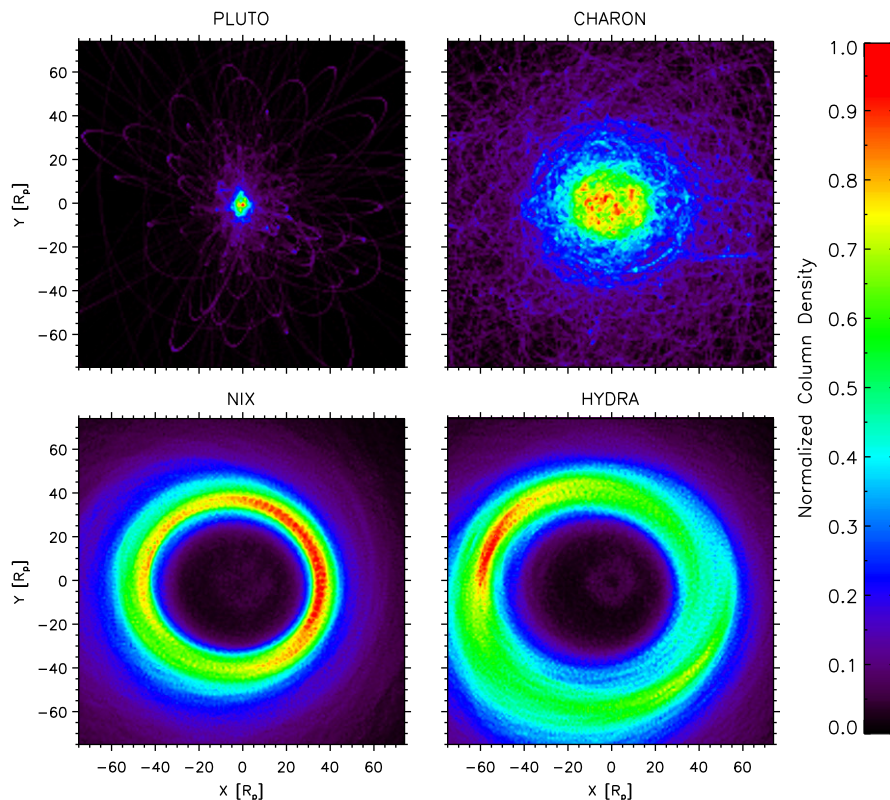


Fig. 4. The column density for each body before appropriate normalization by the dust production rate for 5.0 μm grains. Each panel is normalized to its own maximum column density.

spacecraft upon approach. Nix and Hydra ejecta form tori about their orbital paths, respectively, while Pluto and Charon ejecta form smaller haloes within the Nix and Hydra tori. Fig. 5 shows the model prediction of the net optical depth for all three grain

sizes, respectively, after appropriately normalizing and combining the contribution from all four bodies. Also marked are the orbits of all four bodies (dotted lines) as well as the location at which New Horizons will cross the Pluto–Charon orbital plane. The maximum optical depths at each size are predicted to be $\tau_{0.5} \approx 8.5 \times 10^{-10}$, $\tau_{5.0} \approx 19.4 \times 10^{-9}$, and $\tau_{50.0} \approx 41.7 \times 10^{-8}$, respectively, and in all three cases, Nix and Hydra are the dominant contributor to the optical depth. In the 50.0 μm case, for example, the maximum optical depths for Pluto and Charon are approximately 10^{-10} , while the maximum optical depths from Nix and Hydra are approximately 1×10^{-7} and 4×10^{-7} , respectively. While Nix and Hydra increase the optical depth of grains in the Pluto–Charon system by one to four orders-of-magnitude over previous estimates (Thiessenhusen et al., 2002), we note that the optical depths are still much lower than both the limit set with previous Hubble Space Telescope observations (Steffl and Stern, 2007) as well as an earlier theoretical estimate of the optical depth of $\tau \approx 5 \times 10^{-6}$ (Stern et al., 2006). It should be noted that our calculations are dependent upon a number of parameters that are uncertain and in sum, we suggest that the optical depth estimates quoted above are accurate to an order-of-magnitude.

In mid-2015, the New Horizons spacecraft will fly through the Pluto–Charon system at approximately 12 km/s, crossing at a barycentric distance of approximately 11,000 km ($\approx 9.6R_p$) (Guo and Farquhar, 2008) and passing near the location of peak dust density for the 0.5 μm simulated grains, representing grains between 0.1 and 1.0 μm . The predicted grain flux in this size range in the ram direction along the New Horizons trajectory through the Pluto–Charon system is shown in Fig. 6. Charon-, Nix- and Hydra-generated grains represent approximately equal portions of the impact flux, ranging from approximately $10^{-5} \text{ m}^{-2} \text{ s}^{-1}$ up to $10^{-3} \text{ m}^{-2} \text{ s}^{-1}$. Pluto-generated grains also contribute a small percentage of the flux near the closest approach of New Horizons.

5. Discussion and conclusion

We have addressed the Pluto–Charon dust environment with the inclusion of two newly-discovered moons, Nix and Hydra (Weaver et al., 2006). A previous theoretical analysis was extended to include the presence of Nix and Hydra (Thiessenhusen et al., 2002) and our analysis suggests that these moons contribute roughly equal amounts of ejecta into the Pluto–Charon system,

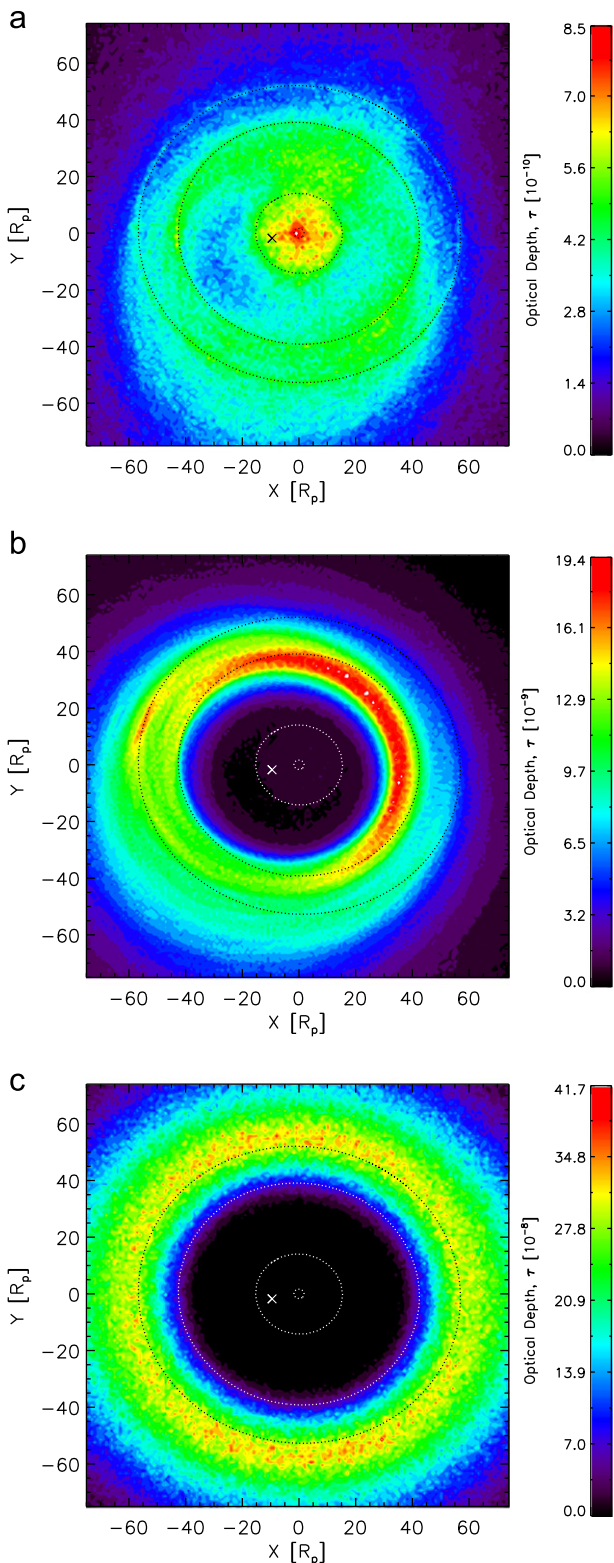


Fig. 5. The geometric optical depth of dust in the Pluto–Charon system from all four bodies for three different grain sizes: (a) 0.5 μm ; (b) 5.0 μm ; (c) 50.0 μm . Also shown are the orbits of all four bodies (dotted lines) and the location at which New Horizons will pass through the Pluto–Charon orbital plane (X). Note the different color scales across plots.

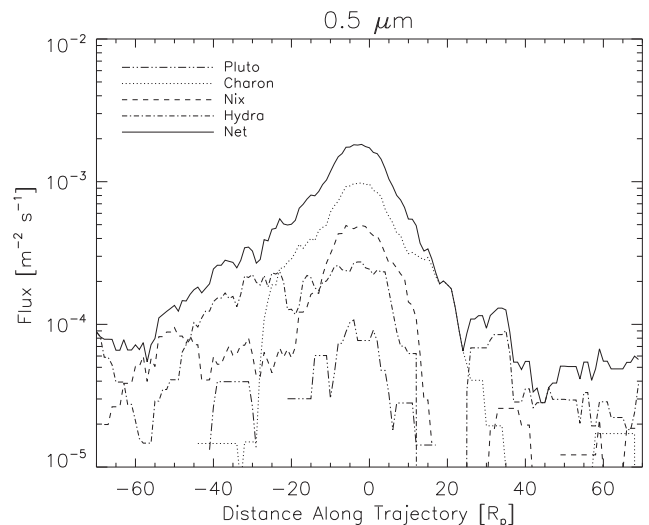


Fig. 6. The flux of $5 \times 10^{-16} \text{ kg}$ (0.5 μm) grains versus along-track distance for a typical New Horizons-like trajectory through the Pluto–Charon system. Shown are curves for the contribution from all four bodies, as well as the net flux.

due to the extremely small escape velocities of the two moons, despite their small cross-section. To model the full dynamics and lifetimes of the ejecta from all four moons, a particle-tracing code was developed and applied to all four bodies. The results showed that Nix- and Hydra-generated grains over a large size range have lifetimes significantly longer than those from Pluto and Charon, which in turn causes Nix and Hydra to be the dominant contributors to the optical depth of grains in the Pluto–Charon system. The optical depths for each grain size from all four bodies combined are lower than an estimate obtained via a different method of $\tau \approx 5 \times 10^{-6}$ for 1.0 μm sized grains (Stern et al., 2006). The discrepancy between these two models is due to the difference in grain lifetimes for Nix and Hydra, which our model predicts to be shorter than that assumed previously. The New Horizons spacecraft will conduct an extensive imaging campaign as it passes through the Pluto–Charon system in mid-2015 and will provide data with which to constrain this model. While the Student Dust Counter on-board New Horizons would have the ability to detect a dust flux of approximately $10^{-3} \text{ m}^{-2} \text{ s}^{-1}$, the instrument will not be operated during the Pluto fly-by due to a variety of operational and scientific constraints. Any detection by New Horizons of a Pluto–Charon dust ring or cloud in excess of this model could suggest active geologic processes from Pluto or its moons, such as cryo-volcanism (Porco et al., 2006). Additionally, just prior to publication of this paper, the discovery of a fourth moon around Pluto, P4, was announced. Smaller than both Nix and Hydra, this tiny moon would also be expected to contribute to the Pluto–Charon dust environment and is a topic of study for future research.

Acknowledgments

This research was supported by the NASA New Horizons mission. The authors thank B. Jacobsmeyer for help in developing the code, E. Grün for helpful discussions and H. Krüger for constructive review comments.

References

- Burns, J.A., Hamilton, D.P., Showalter, M., 2001. Dusty rings and circumplanetary dust. In: Grün, E., Gustafson, B.A.S., Dermott, S., Fechtig, H. (Eds.), *Interplanetary Dust*. Springer.
- Burns, J.A., Lamy, P.L., Soter, S., 1979. Radiation forces on small particles in the solar system. *Icarus* 40, 1–48.
- Burns, J.A., Showalter, M., Hamilton, D.P., Nicholson, P.D., de Pater, I., Ockert-Bell, M.E., Thomas, P.C., 1999. The formation of Jupiter's faint rings. *Science* 284, 1146–1150.
- Cruikshank, D.P., Bell, J.F., Gaffey, M.J., Brown, R.H., Howell, R., Beerman, C., Rognstad, M., 1983. The dark side of Iapetus. *Icarus* 53, 90–104.
- Delamere, P.A., 2009. Hybrid code simulations of the solar wind interaction with Pluto. *Journal of Geophysical Research* 114, A03220.
- Delamere, P.A., Bagenal, F., 2004. Pluto's kinetic interaction with the solar wind. *Geophysical Research Letters* 31 (L04807).
- Frisch, W., 1992. Hypervelocity impact experiments with water ice targets. In: McDonnell, J.A.M. (Ed.), *Hypervelocity Impacts in Space*. Univ. of Kent, Canterbury.
- Grün, E., Zook, H.A., Fechtig, H., Giese, R.H., 1985. Collisional balance of the meteoric complex. *Icarus* 62, 244–272.
- Guo, Y., Farquhar, R.W., 2008. New Horizons mission design. *Space Science Review* 140, 49–74.
- Hamilton, D.P., Burns, J.A., 1994. Origin of Saturn's E ring: self-sustained, naturally. *Science* 264, 550–553.
- Harnett, E.M., Winglee, R.M., Delamere, P.A., 2005. Three-dimensional multi-fluid simulations of Pluto's magnetosphere: a comparison to 3D hybrid simulations. *Geophysical Research Letters* 32 (L19104).
- Hartmann, W.K., 1985. Impact experiments: 1. Ejecta velocity distributions and related results from regolith targets. *Icarus* 63, 69–98.
- Hedman, M.M., Murray, C.D., Cooper, N.J., Tiscareno, M.S., Beurle, K., Evans, M., Burns, J.A., 2009. Three tenuous rings/arcs for three tiny moons. *Icarus* 199, 378–386.
- Hendrix, A.R., Hansen, C.J., 2008. The albedo dichotomy of Iapetus measured at UV wavelengths. *Icarus* 193, 344–351.
- Horányi, M., et al., 2008. The Student Dust Counter on the New Horizons mission. *Space Science Review* 140, 387–402.
- Humes, D.H., 1980. Results of Pioneer 10 and 11 meteoroid experiments: interplanetary and near-Saturn. *Journal of Geophysical Research* 85 (A11), 5841–5852.
- Ip, W.-H., Banaszkiewicz, M., 1990. On the dust/gas tori of Phobos and Deimos. *Geophysical Research Letters* 17 (6), 857–860.
- Juhász, A., Horányi, M., 1995. Dust torus around Mars. *Journal of Geophysical Research* 100 (E2), 3277–3284.
- Koschny, D., Grün, E., 2001a. Impacts into ice-silicate mixtures: crater morphologies, volumes, depth-to-diameter ratios, and yield. *Icarus* 154, 391–401.
- Koschny, D., Grün, E., 2001b. Impacts into ice-silicate mixtures: ejecta mass and size distributions. *Icarus* 154, 402–411.
- Krivov, A.V., Krüger, H., Grün, E., Hamilton, D.P., 2002. A tenuous dust ring of Jupiter formed by escaping ejecta from the Galilean satellites. *Journal of Geophysical Research* 107 (E1).
- Krivov, A.V., Sremčević, M., Spahn, F., Dikarev, V.V., Kholshvnikov, K.V., 2003. Impact-generated dust clouds around planetary satellites: spherically symmetric case. *Planetary and Space Science* 51, 251–269.
- Krüger, H., Krivov, A.V., Grün, E., 2000. A dust cloud of Ganymede maintained by hypervelocity impacts of interplanetary micrometeoroids. *Planetary and Space Science* 48 (5), 1457–1471.
- Krüger, H., Krivov, A.V., Hamilton, D.P., Grün, E., 1999. Detection of an impact-generated dust cloud around Ganymede. *Nature* 399 (June).
- Landgraf, M., et al., 2002. Origins of solar system dust beyond Jupiter. *Astronomical Journal* 123, 2857–2861.
- McComas, D., Allegrini, F., Bagenal, F., Casey, P., Delamere, P., Demkee, D., Dunn, G., Elliott, H., Hanley, J., Johnson, K., Langle, J., Miller, G., Pope, S., Reno, M., Rodriguez, B., Schwadron, N., Valek, P., Weidner, S., 2008. The Solar Wind Around Pluto (SWAP) instrument aboard New Horizons. *Space Science Review* 140, 261–313.
- Poppe, A., James, D., Jacobsmeyer, B., Horányi, M., 2010. First results from the Venetia Burney Student Dust Counter on the New Horizons mission. *Geophysical Research Letters* 37 (June).
- Porco, C.C., et al., 2005. Cassini imaging science: initial results on Phoebe and Iapetus. *Science* 307, 1237–1242.
- Porco, C.C., et al., 2006. Cassini observes the active south pole of Enceladus. *Science* 311 (March), 1393–1401.
- Spencer, J.R., Stansberry, J.A., Trafton, L.M., Young, E.F., Binzel, R.P., Croft, S.K., 1997. Volatile transport, seasonal cycles, and atmospheric dynamics on Pluto. In: Stern, D.J., Tholen, D.J. (Eds.), *Pluto and Charon*. University of Arizona Press, pp. 435–473.
- Steffl, A.J., Mutchler, M.J., Weaver, H.A., Stern, S.A., Durda, D.D., Terrell, D., Merline, W.J., Young, L.A., Young, E.F., Buie, M.W., Spencer, J.R., 2006. New constraints on additional satellites of the Pluto system. *Astronomical Journal* 123, 614–619.
- Steffl, A.J., Stern, S.A., 2007. First constraints on rings in the Pluto system. *Astronomical Journal* 133, 1485–1489.
- Stern, S.A., 2008. The New Horizons Pluto Kuiper Belt Mission: an overview with historical context. *Space Science Review* 140, 3–21.
- Stern, S.A., 2009. Ejecta exchange and satellite color evolution in the Pluto system, with implications for KBOs and asteroids with satellites. *Icarus* 199, 571–573.
- Stern, S.A., Trafton, L.M., Gladstone, G.R., 1988. Why is Pluto bright? Implications of the albedo and lightcurve behavior of Pluto. *Icarus* 75, 485–498.
- Stern, S.A., Weaver, H.A., Steffl, A.J., Mutchler, M.J., Buie, W.M., Merline, W.J., Young, E.F., Young, L.A., Spencer, J.R., 2006. A giant impact origin for Pluto's small moons and satellite multiplicity in the Kuiper belt. *Nature* 439.
- Stöffler, D., Gault, D.E., Wedekind, J., Polkowski, G., 1975. Experimental hypervelocity impact into quartz sand: distribution and shock metamorphism of ejecta. *Journal of Geophysical Research* 80 (29).
- Thiessenhusen, K.-U., Krivov, A.V., Krüger, H., Grün, E., 2002. A dust cloud around Pluto and Charon. *Planetary and Space Science* 50, 79–87.
- Tholen, D.J., Buie, M.W., Grundy, W.M., Elliott, G.T., 2008. Masses of Nix and Hydra. *Astronomical Journal* 135, 777–784.
- Verbischer, A.J., Skrutskie, M.F., Hamilton, D.P., 2009. Saturn's largest ring. *Nature* 461.
- Weaver, H.A., Stern, S.A., Mutchler, M.J., Steffl, A.J., Buie, M.W., Merline, W.J., Spencer, J.R., Young, E.F., Young, L.A., 2006. Discovery of two new satellites of Pluto. *Nature* 439, 943–945.